Article

Not peer-reviewed version

A DNA-Based Plasmonic Nano-Ruler

Aura Cencini , Mary Bortoluzzi , Graziano Rilievo , Federica Tonolo , Fabio Vianello , Massimiliano Magro * , Alessandro Cecconello

Posted Date: 4 February 2025

doi: 10.20944/preprints202502.0204.v1

Keywords: DNA nanotechnologies; self-assembly; plasmonic nanoparticles; fluorescence; quenching-enhancing

 doi:10.20944/preprints202502.0204.v1

Article

A DNA-Based Plasmonic Nano-Ruler

Aura Cencini [1], Mary Bortoluzzi [1], Graziano Rilievo [1], Federica Tonolo [1], Fabio Vianello [1], Massimiliano Magro [1,*] and Alessandro Cecconello [1]

Department of Comparative Biomedicine and Food Science, University of Padua, Viale dell'Università 16, 35020, Legnaro (PD), Italy

* Correspondence: massimiliano.magro@unipd.it; Tel.: +39-(0)49-8272916

Abstract: DNA is an exceptional building block for the fabrication of dynamic supramolecular systems with switchable geometries. Here, a self-assembled, tunable plasmonic-fluorescent nanostructure was developed. A precise sliding motion mechanism was operated through the control of strand displacement reactions, shifting two single-strand DNA (ssDNA) rails connected by a ssDNA quasi-ring structure. The system was reconfigured as a nano-mechanical structure, generating six discrete configurations, and setting specific distances between a tethered gold nanoparticle (AuNP) and a fluorophore (Cy3). Each configuration produced a distinct fluorescence emission intensity via plasmonic quenching/enhancement effects, and therefore the structure behaved as a nano-ruler. To optimize the system, the reversible distance-dependent fluorescence quenching or enhancement phenomena were investigated by testing gold nanoparticles with diameters 5, 10, and 15 nm, yielding the best performances with 10 nm AuNPs. Furthermore, a geometric model of the system was produced, confirming the observed results. The fluorophore-plasmonic surface positioning, conferred by the DNA ruler, led to a finite state nano-machine with six alternative signal outputs. This mechanism, working as a fluorescent reporter, could find application in a multiple-responsive detection system of single-strand nucleic acids, such as viruses or miRNAs.

Keywords: DNA nanotechnologies; self-assembly; plasmonic nanoparticles; fluorescence; quenching-enhancing

1. Introduction

DNA has been extensively used to tailor functional supramolecular systems using Watson–Crick or analogue simple base-pairing rules [1]. In the boundless scenario of DNA technology, machine-like dynamic assemblies, that can be structurally switched in a programmable way, stand out for their potential of exerting a punctual control over matter through the generation of structures and mechanical forces at an actual nanosize level [2–4]. In this view, a kaleidoscope of artificial DNA structure-based applications is available in literature nowadays. Among them, DNA-based nanoscale templating of inorganic objects [5], multi-responsive DNA hydrogels [6], and other DNA-based nano-machines [7–9], was carried out through self-assembly or mechanically "fuelled" designs. This consists in using ssDNA not only as a structural material but also as a `fuel', namely auxiliary single strand strands of DNA are added to the solution to induce motion through conformational changes and, as a molecular motor, each cycle produces duplex DNA as a waste product [10]. Such DNA-based nano-mechanical structures, that can be reversibly opened and closed in a programmed way, were applied to develop finite-state machines and logic gates [11], paving the way for DNA computing[12] and storage systems [13–15].

Fluorescence-based nanotechnologies, that commonly found application in a wide range of scenarios, ranging from biosensing to in vivo imaging [16–19], were successfully used as reporting systems for the reconfigurations of DNA-based machines [20]. In this context, aiming at improving the limit of detection and to expand the choice of fluorophores, continuous efforts were dedicated to

 doi:10.20944/preprints202502.0204.v1

the enhancement of fluorescence intensity [21]. Indeed, among different approaches, molecular fluorescence could be modulated through the vicinity of a metal nano-surface, resulting in emission quenching at short distances or emission enhancement farther away from the surface and at a precise distance range [22]. Theoretical analyses demonstrated that several parameters including metal type, fluorophore dipole orientation, and nanoparticle shape are key players, besides surface-fluorophore distance, for manipulating fluorescence [23]. In recent years, DNA origami nano-rulers for super-resolution (SR) fluorescence microscopy have evolved from experimental *proof-of-concepts* to commercially available benchmarks [24]. These self-assembled nanostructures are dynamic supramolecular systems that are obtainable with high reproducibly and high yields, arranging a defined number of fluorophore molecules within programmed nano-sized architectures. Furthermore, the requirement of a molecular frame for the precise positioning of nanoparticles and fluorophores was explored by the tailored assembly of DNA-scaffolded metal nanoparticle/fluorophore nanostructures in one- [25], two- [26], or three-dimensional structures [27].

Here, a novel DNA actuator was explored combining (i) the ability of DNA as building block to develop dynamic nano-machines and (ii) the effect of noble metal nanoparticles on a fluorophore optical properties. The DNA structure behaved as a six-state dynamic spacer comprising a DNA-functionalized single fluorophore (Cy3) and a single DNA-modified AuNP, tethered to sterically dictated positions via sequence-specific DNA duplex formation. The functionalized parts were designed to "slide" over each other, shortening or extending the fluorophore-AuNP separating distance by strand-displacement mechanism-triggered reconfigurations, therefore affecting fluorescence emission.

10 nm gold nanoparticles emerged as the ideal plasmonic counterpart for the fine-tuning of the Cy3 fluorescence while the reversibility of the fluorescence quenching/enhancement phenomena upon DNA-based motion mechanisms was demonstrated by recording fluorescence emission during the strand displacement-triggered scaffold reconfigurations. Six discrete fluorophore-AuNP distances and as many specific fluorescence signals highlighted the feasibility of the complex assembly as a finite-state fluorescent nano-device providing information on the fluorophore-AuNP separating distance via fluorescence emission and thus behaving as a nano-ruler.

2. Results

The positioning of nano-objects at close relative distances relies on the ability to precisely control their chemical connectivity. DNA allows the dictated control over the formation of sequence-specific duplexes, which in this study was used to determine the location of a fluorophore with sub-nanometer precision. On the other hand, to ensure the attachment on the scaffold of individual AuNPs and avoid crosstalk with other DNA components or multiple bindings, single DNA-functionalized particles are necessary, i.e., monovalent particles. This was obtained via thiol-gold chemistry using an -SH modified oligonucleotide (see table S1, SI, for a list of the DNA strands), and by electrophoretic separation and purification of the monovalent product. To optimize the system as a fluorescence reporter, the effects of 5, 10, and 15 nm diameter AuNPs on a fluorophore (Cy3) optical properties were investigated. For simplicity, the results section is dedicated to the description of the best configuration of the system, with 10 nm-AuNPs. A brief comparison of the 10 nm AuNP effects with the 5 and 15 nm AuNP-DNA hybrid assemblies is commented at the end of the section.

Figure 1(a) shows a scheme of the thiolated-DNA functionalization process and an exemplary gel electrophoretic separation of the DNA-functionalized 10nm AuNPs, where bands corresponding to 1-, 2-, and 3-strand functionalized particles are visible at increasing thiol-DNA/AuNP molar ratio. Once the band of interest was excised from the agarose gel, the particles were collected in a dialysis tube and cleaned in TBE buffer (a complete description of the AuNP modification, separation, and purification is reported in the method section, while additional details are reported in the SI).

The self-assembled dynamic DNA structure generating the nano-ruler comprises AuNP-modified Rail A, i.e., partial duplex (1)/(2), the roller ssDNA quasi-ring strand (3), and Rail B, i.e., Cy3-functionalized ssDNA (4) or (5). The structure exists in six configurations: States S1, S2, and S3,

 doi:10.20944/preprints202502.0204.v1

carrying a Cy3 functionality internal to strand (4). Replacing strand (4) with strand (5), states S4, S5, and S6 are realized where Cy3 fluorophore is positioned at the 3′ end of strand (4). The dynamic reconfigurations are operated by additional strands (6), (7), and (8) and their respective complementary strands (6*), (7*), and (8*) via toehold-assisted strand-displacement mechanism. Strands (9) and (10) rigidify the structure, limiting the oscillations and allowing for precise fluorophore-plasmonic surface positioning. Figure 1(b) shows a stepwise scheme of the DNA structure self-assembly.

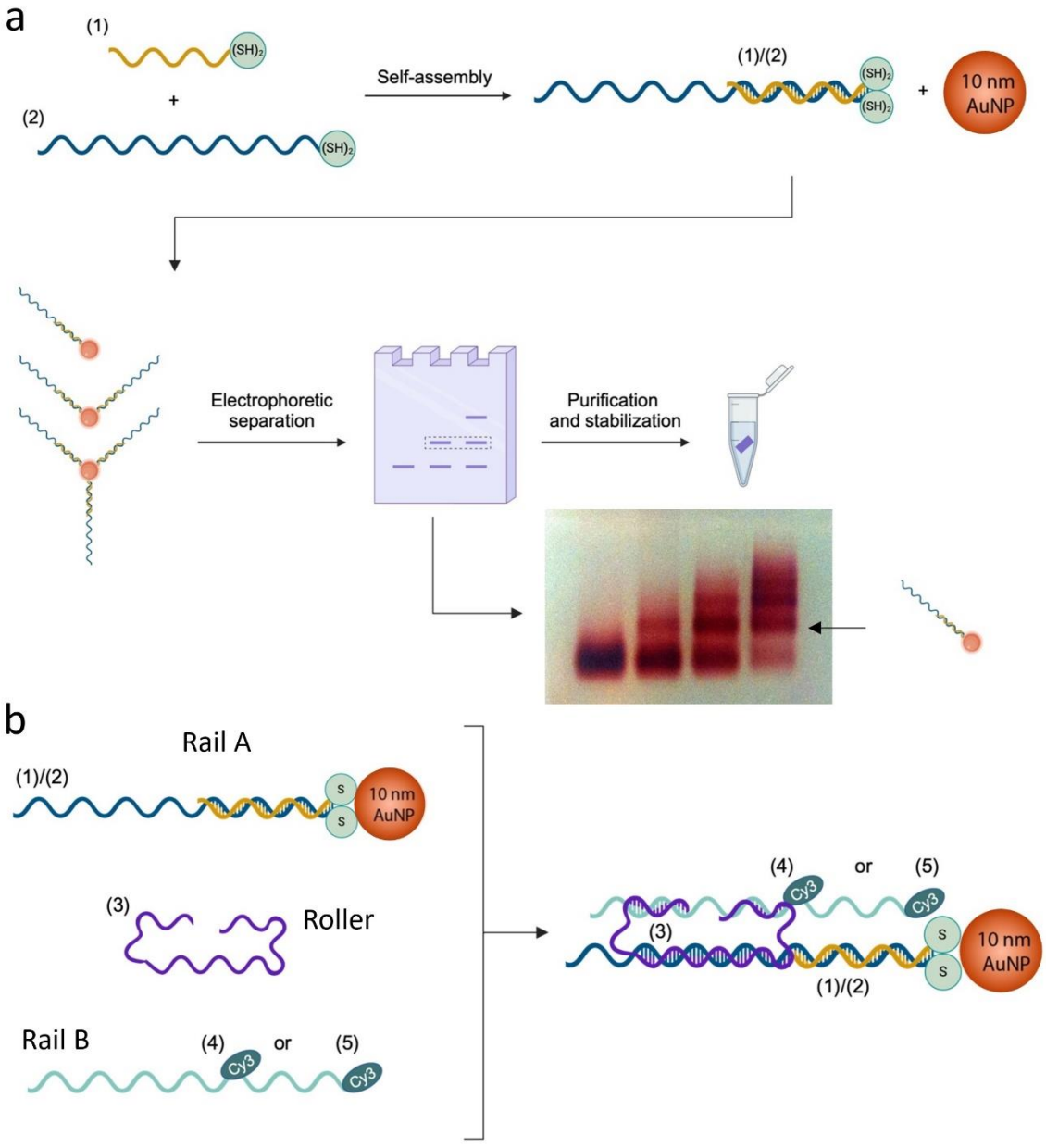

Figure 1. DNA slider assembly scheme. (a) production of single DNA-functionalized 10 nm AuNP and a representative agarose gel electrophoretic separation. (b) Stepwise assembly scheme of the slider DNA scaffold.

Once the slider was assembled, its reconfigurations were monitored in a quartz cuvette by fluorescence emission changes (λ= 565 nm) upon addition of a small excess of the appropriate strand (for the details of the reconfiguration operations, including concentrations and volumes of all mixtures, see the methods section and the SI). A scheme of the slider reconfigurations across states S1, S2, and S3 is reported in Figure 2(a) along with the respective fluorescence emission changes in Figure 2(b). At first, the slider was locked in state S1 by strand (6) and rigidifying helper strand (9).

Preprints.org (www.preprints.org) | NOT PEER-REVIEWED | Posted: 4 February 2025 doi:10.20944/preprints202502.0204.v1

In this state, Cy3 is the farthest from the AuNP surface and near-field phenomena are highly inefficient. We set this emission intensity as the normalizing value, as reported in Figure 2(b) plot. Upon addition of complementary strand (6*) and strand (7), strand (6) is removed by formation of the more stable duplex (6)/(6*), while strand (7) locks the slider in state S2. Here, the fluorophore is the closest to the AuNP surface and the respective fluorescence signal reaches a minimum. Next, state S1 is restored by adding removal strand (7*) and strand (6). In the following step, when strands (6*) and (8) are added to the mixture, the slider reconfigures to state S3, bringing Cy3 at an intermediate distance from the AuNP and the associated fluorescence emission reaches a maximum. Finally, state S1 is restored by adding removal strand (8*) and strand (6), for the complete scheme of state transitions and associated reconfiguration strands, see appropriate section of the SI. The slider was cycled one more time across states S2, S1, and S3, showing a near perfect reproducibility of the first cycle emission levels, Figure 2(b).

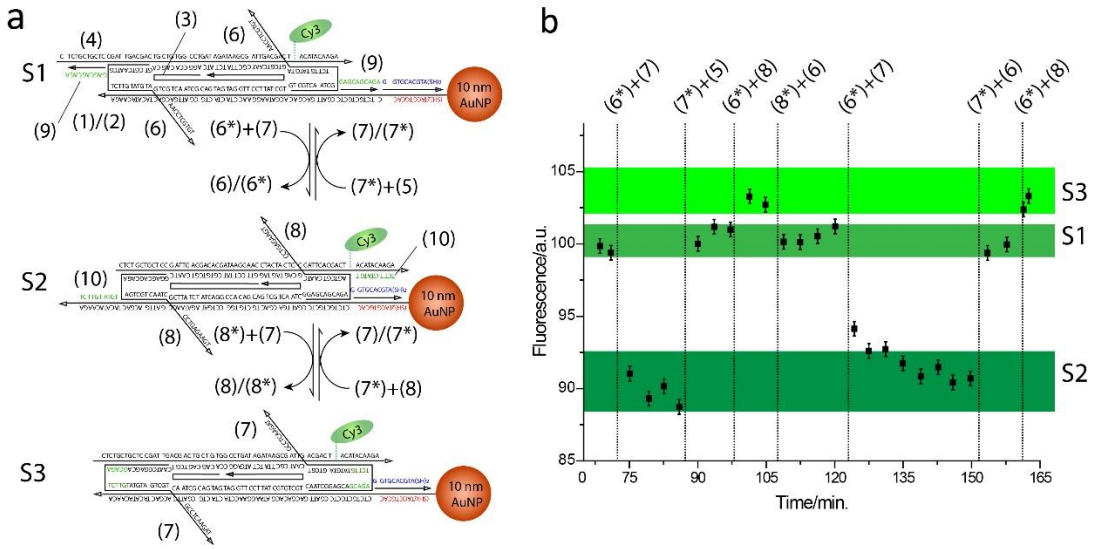

Figure 2. Mechanical control of the fluorescence properties of the DNA slider through strand displacement reactions. (a) three discrete configurations S1, S2, and S3 were obtained, generating three specific Cy3-AuNP separating distances. (b) fluorescence emission levels recorded at (λ= 565 nm) associated with the slider reconfigured across states S1, S2, S1, S3, S1, S2, S1, S3.

Next, a slider where Rail B strand (4) was replaced with strand (5) was assembled and characterized, similarly to the first slider. Here, Cy3 is positioned at the 3′ of strand (5) and therefore the slider reconfigurations are expected to generate structures with shorter Cy3-AuNP separating distances. Figure 3(a) shows a scheme of the slider reconfigurations across states S4, S5, and S6 along with the associated fluorescence emission levels, Figure 3(b). The slider was initially locked in state S4 by strand (6) and the stepwise addition of strands (6*)+(7) and (7*)+(8) reconfigured the slider to states S5 and S6, respectively. Fluorescence emission levels were progressively reduced, indicating quenching phenomena as Cy3-AuNP separating distance became shorter. In addition, as previously observed, the slider was re-set to state S1 and cycled again through states S2, S3, and S1, showing results analogous to the first cycle.

Preprints.org (www.preprints.org) | NOT PEER-REVIEWED | Posted: 4 February 2025 doi:10.20944/preprints202502.0204.v1

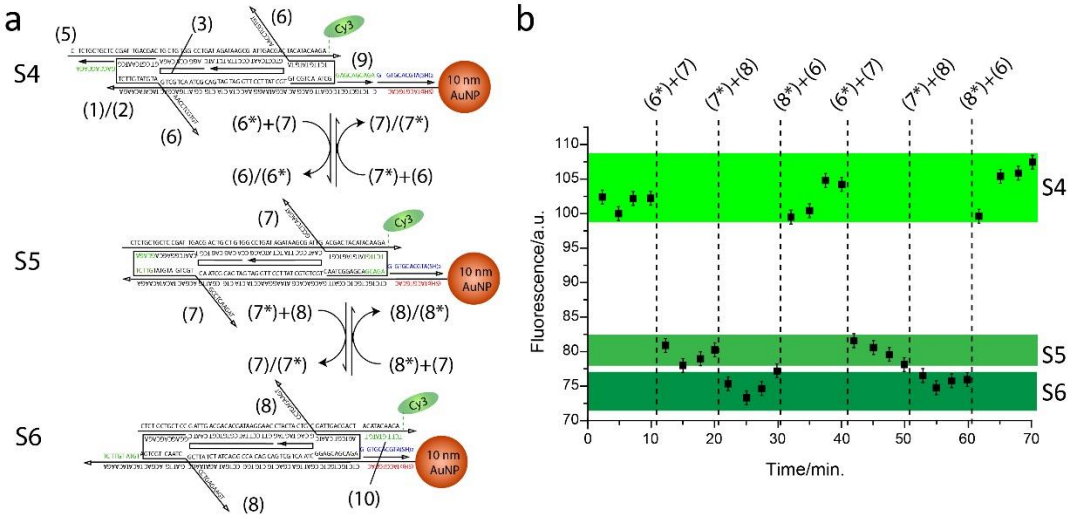

Figure 3. Mechanical control of the fluorescence properties of the nanoruler through strand displacement reactions. (a) three discrete configurations S4, S5 and S6 were obtained, generating three specific Cy3-AuNP separating distances. (b) fluorescence emission levels recorded at (λ= 565 nm) associated with the slider reconfigured across states S4, S5, S6, S4, S5, S6, S4.

[28] For comparison, 5 and 15 nm AuNP nano-rulers were assembled, and the characteristic fluorescence emission levels were recorded at the different structure states. 5 nm AuNPs were ruled out as they gave rise to a negligible enhancement effect, likely ascribable to their small size (data not shown). On the contrary, the larger 15 nm AuNPs were not suitable for this molecular configuration as witnessed by their imprecise quenching-enhancement responses (Figure s1, SI). This can be attributed to the nanoparticle diameter, comparable to the broader shift of the current system, making impossible a fine-positioning in the range of distances set by the DNA slider. These outcomes suggest that an adequately dimensioned design is required for matching with the steric hindrance of 15 nm, probably needing a bulkier DNA scaffold that would prevent particle oscillations. Hence, 10 nm AuNPs emerged as the optimal metal counterpart for fabricating a fluorophore-plasmon surface distance-depending finite state nanomachine, potentially applicable as multi-responsive fluorescent reporter for in vitro tests.

3. Discussion

Fluorescence imaging and sensing have greatly benefited from the integration of surface plasmon resonance, yielding a number of surface plasmon-assisted fluorescence tools with noteworthy applications such as, among the others, the real-time visualization of biomolecules in vivo. [28]

Here, we developed a real-time reporter of single-strand nucleic acid, such as virus or miRNA using a fine-tunable plasmonic-fluorescent nano-ruler. Indeed, target single-strand nucleic acids can be detected through strand displacement reactions with complementary sequences in the ruler, inducing the precise sliding motion of two ssDNA rails over a ssDNA quasi-ring structure. This mechanism operates a fine-tuning of the distance separating a 10 nm gold nanoparticle and a fluorophore unit (Cy3), with an effect on Cy3 fluorescence that ranges from quenching to enhancement, generating six discrete signal outputs. The Cy3 fluorescence enhancement can be explained recalling the concept of plasmon-enhanced fluorescence that is a condition by which a resonance involves the fluorophore emission frequency and the metal nanoparticle plasmon resonance. As a result, because of elastic scattering, an amplified emission at the same frequency as that of the organic fluorophore will be attained. For this purpose, the absorption/emission profile of the fluorophore must significantly overlap with one of the optical features of the metal nanoparticle.

 doi:10.20944/preprints202502.0204.v1

[28,29] Moreover, the phenomenon strongly depends on the shape, size, and separation distance as observed herein. On the other hand, quenching can be ascribed to the instant energy transfer from the excited state of the fluorophore to the peripheral conduction electrons of the metal nanoparticle. The quenching is dependent on the donor-to-acceptor distance and occurs when a fluorophore is positioned at a distance below 10 nm from the plasmonic surface as in the present case. [28]

To address the different emission levels, we used geometrical considerations to calculate the expected Cy3-AuNP distances for the different states. Figure 4, panels (b) and (d), show a geometric scheme of the different separating distances reporting values equal to 1, 3, 5, 6, 7, and 10 nm associated with states S6, S5, S4, S2, S3, and S1. These values were compared to theoretical enhancing/quenching effects using a published model [30], Figure 4, panels (a) and (c). Indeed, results are in good agreement with the model, confirming the correct assumptions for the geometric considerations.

4. Materials and Methods

A detailed description of the steps required to assemble the nano-ruler is presented in the SI. Briefly, thiolated synthetic DNA oligonucleotides (Integrated DNA Technologies, Coralville, USA) were reacted with AuNPs to obtain the conjugate AuNP-DNA. Electrophoretically separated (Lonza, small-nucleotide separating 2% agarose; separation carried out in ice at low voltage) single-DNA carrying AuNPs were then used to self-assemble by temperature ramp the nano-ruler, comprising a Cy3-modified oligonucleotide. The final complex was operated at a concentration of 50 nM with a small excess of reconfiguring strands.

Theoretical calculation correlating the distance-dependent fluorescence quantum yields of the Cy3 fluorophore in the Au NPs-rotaxane dumbbell structure. The fluorescence features of Cy3 in the different configurations of the Au NPs(10nm)/DNA/Cy3 hybrid rotaxane system were simulated theoretically by using an on-line, free available software [30]. We attempted to theoretically calculate the fluorescence quantum yields of Cy3 as a function of the distance separating the fluorophore from the NP surface. In order to do that, the following parameters were adopted in the software-assisted calculations: - equal diameter: 10 nm S8 - prolate aspect ratio: 1 -metal: Au -medium index: 1.3 - X-axis distance: 0-30 nm - wavelength: 560 - dipole orientation: perpendicular -reference QE: 0.01 - method: Gersten -radiative damping: yes - dynamic depolarization: yes - angular mode numbers lstart: 1; leval: 0 and lcut: 60. The final plots are shown in Figure 4, panels (a) and (c), where a maximum enhancement (20%) is predicted at a separating distance of ca. 8 nm and the quenching area is positioned in the separating distance interval of 0-5.4 nm.

Preprints.org (www.preprints.org) | NOT PEER-REVIEWED | Posted: 4 February 2025 doi:10.20944/preprints202502.0204.v1

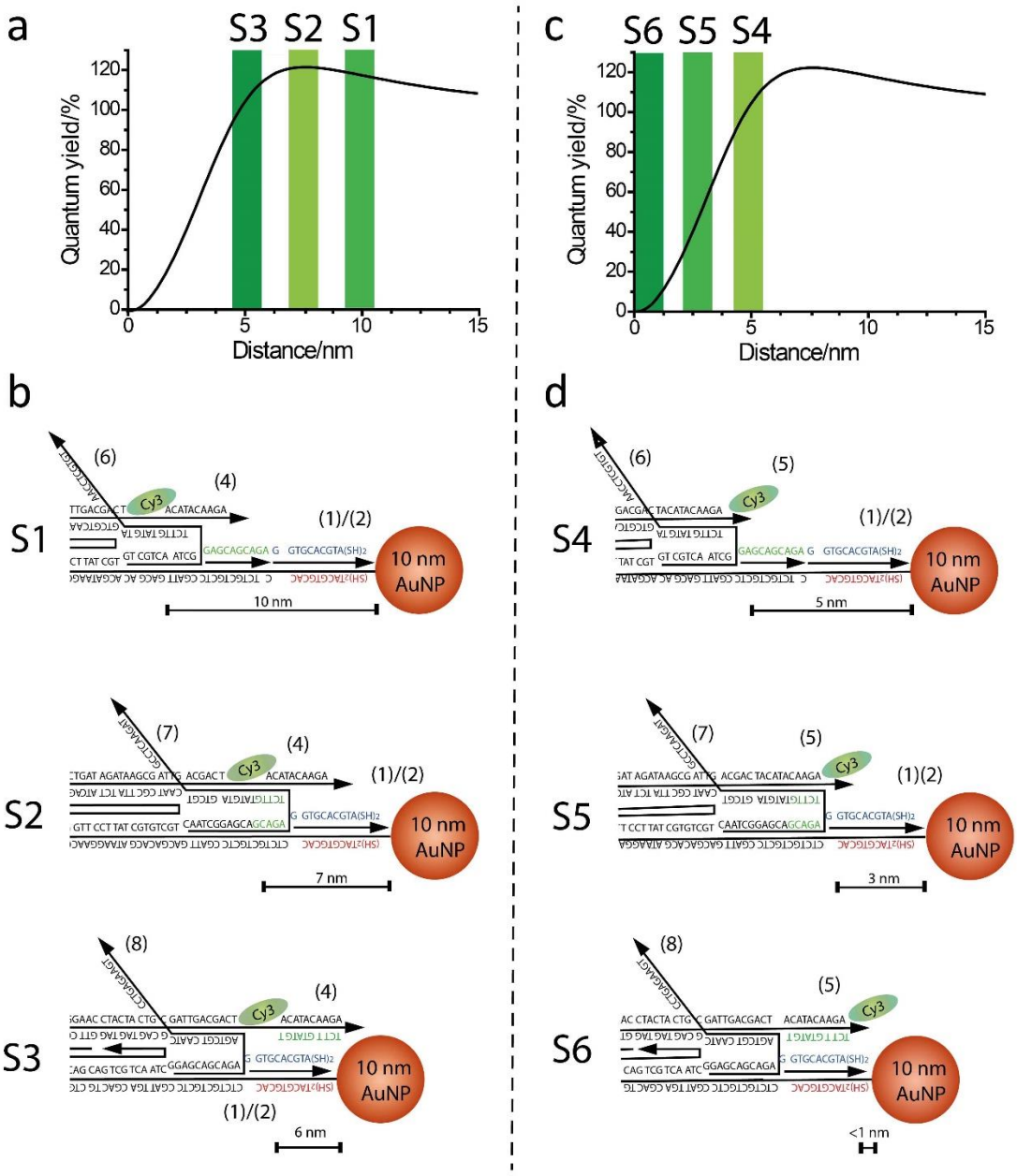

Figure 4. Comparison of experimental and theoretical quenching/enhancement effects. (a), (c) theoretical model of the distance-dependent quenching/enhancing effects of a plasmonic surface on Cy3 fluorescence emission according to [30] .(b), (d) scheme of the geometric distances separating Cy3 and the 10 nm AuNP, as calculated considering the DNA scaffold sizes.

5. Conclusions

Fluorescent DNA nano-rulers are dynamic supramolecular systems, permitting to configure a defined number of fluorophores in programmed nano-sized architectures. Herein, the optimization of a switchable DNA nano-machine able to the cyclic and reversible transition between discrete fluorescent states was described. The supramolecular self-assembly consists of a quasi-circular ring acting as support for two sliding ssDNA rails, which programmed motion varies the distance between a gold nanoparticle and a Cy3 fluorophore. In order to obtain an actual fine-tunable fluorescent emitter 5, 10, and 15 nm nanoparticles were screened, identifying 10 nm as the optimal AuNPs size displaying the best dynamic range, both in terms of quenching and enhancement. The movements are generated by strand displacement reactions, due to complementary sequences that

 doi:10.20944/preprints202502.0204.v1

are present in the milieu, hence the system can be used as a fluorescent reporter for single strand nucleic acids such as RNA viruses.

Supplementary Materials: The following supporting information can be downloaded at the website of this paper posted on Preprints.org, Materials, Table S1: Sequences of the core structure oligonucleotides; Table S2. Sequences of the operating and rigidifying oligonucleotides. Star-signs indicate complementary sequences; additional methods for the single oligonucleotide-modified AuNPs, their stabilization, and the theoretical calculations correlating the distance-dependent fluorescence quantum yields of the Cy3 fluorophore in the AuNP-functionalized nano-ruler structure.

Author Contributions: Conceptualization: AuC, AlC; Data curation: AuC, MB, GR, AlC,; Formal analysis: AuC, FT; Funding acquisition: FV, AlC; Investigation: AuC GR, FT; Methodology: AuC, GR, AlC; Project administration: FV,MM,; Resources: FV, MM, AlC,; Software: GR; Supervision: FV, MM, AlC; Writing – original draft: AuC, MM, AlC; Writing – editing: AuC, MB, GR, FT, FV, MM, AlC; Visualization: MB.

Funding: Federica Tonolo was supported by "iNEST- Interconnected Nord-Est Innovation ECS00000043" and PNRR Young Researchers Project "CirculaR EConomy to enhance the sustainabilitY of agri-food Chain: An innovative approach to transform food wastE into functionaL foods". Aura Cencini was supported by the Italian Ministry of Education, University and research (MIUR) funds "Sentinel". Alessandro Cecconello was supported by REACT-EU PON "Ricerca e Innovazione 2014–2020" and Supporting TAlents in ReSeach (STARS@UNIPD 2023).

Conflicts of Interest: The authors declare no conflicts of interest.

Abbreviations

The following abbreviations are used in this manuscript:

AuNP	Gold nanoparticle
Cy3	Sulfo-Cyanine3

References

1. Mao, X.; Liu, M.; Li, Q.; Fan, C.; Zuo, X. DNA-Based Molecular Machines. *JACS Au* 2022, *2*.
2. Hu, Y.; Ying, J.Y. Reconfigurable A-Motif, i-Motif and Triplex Nucleic Acids for Smart PH-Responsive DNA Hydrogels. *Materials Today* 2023, *63*.
3. Mills, A.; Aissaoui, N.; Maurel, D.; Elezgaray, J.; Morvan, F.; Vasseur, J.J.; Margeat, E.; Quast, R.B.; Lai Kee-Him, J.; Saint, N.; et al. A Modular Spring-Loaded Actuator for Mechanical Activation of Membrane Proteins. *Nat Commun* **2022**, *13*, doi:10.1038/s41467-022-30745-2.
4. Benson, E.; Carrascosa Marzo, R.; Bath, J.; Turberfield, A.J. Strategies for Constructing and Operating DNA Origami Linear Actuators. *Small* **2021**, *17*, 2007704, doi:10.1002/smll.202007704.
5. Michelson, A.; Subramanian, A.; Kisslinger, K.; Tiwale, N.; Xiang, S.; Shen, E.; Kahn, J.S.; Nykypanchuk, D.; Yan, H.; Nam, C.Y.; et al. Three-Dimensional Nanoscale Metal, Metal Oxide, and Semiconductor Frameworks through DNA-Programmable Assembly and Templating. *Sci Adv* **2024**, *10*, doi:10.1126/sciadv.adl0604.
6. Rui Lee, S.; Yu Jie Ong, C.; Yi Wong, J.; Ke, Y.; Dong, Z.; Lim, J.Y.C.; Hu, Y. Supramolecular Oligo-Thymine/Melamine Nanobridge-Driven Macroscopic Engineering: Reprogrammable Hydrogels for Multi-Stimuli Responsive Architectures. *Chemical Engineering Journal* **2024**, *497*, 154698, doi:10.1016/j.cej.2024.154698.
7. Rothfischer, F.; Vogt, M.; Kopperger, E.; Gerland, U.; Simmel, F.C. From Brownian to Deterministic Motor Movement in a DNA-Based Molecular Rotor. *Nano Lett* **2024**, *24*, 5224–5230, doi:10.1021/acs.nanolett.4c00675.
8. Hildebrandt, L.L.; Preus, S.; Zhang, Z.; Voigt, N. V.; Gothelf, K. V.; Birkedal, V. Single Molecule FRET Analysis of the 11 Discrete Steps of a DNA Actuator. *J Am Chem Soc* **2014**, *136*, doi:10.1021/ja502580t.

9. Zhang, Z.; Olsen, E.M.; Kryger, M.; Voigt, N. V.; TØrring, T.; Gültekin, E.; Nielsen, M.; Mohammadzadegan, R.; Andersen, E.S.; Nielsen, M.M.; et al. A DNA Tile Actuator with Eleven Discrete States. *Angewandte Chemie - International Edition* **2011**, *50*, doi:10.1002/anie.201007642.
10. Simmel, F.C.; Yurke, B.; Singh, H.R. Principles and Applications of Nucleic Acid Strand Displacement Reactions. *Chem Rev* 2019, *119*.
11. Wang, K.; Huang, Q.; Elshaer, M.R.; Knorr, B.; Chaikin, P.; Zhu, G. Tri-State Logic Computation by Activating DNA Origami Chains. *Nanoscale* **2024**, *16*, 11991–11998, doi:10.1039/D3NR06010A.
12. Lilienthal, S.; Klein, M.; Orbach, R.; Willner, I.; Remacle, F.; Levine, R.D. Continuous Variables Logic via Coupled Automata Using a DNAzyme Cascade with Feedback. *Chem Sci* **2017**, *8*, 2161–2168, doi:10.1039/C6SC03892A.
13. Soukarie, D.; Nocete, L.; Bittner, A.M.; Santiago, I. DNA Data Storage in Electrospun and Melt-Electrowritten Composite Nucleic Acid-Polymer Fibers. *Mater Today Bio* **2024**, *24*, doi:10.1016/j.mtbio.2023.100900.
14. Zhong, W.; Wang, S.; Geng, C.; Zheng, Y.; Bai, S.; Cao, X.; Liu, K.; Yang, Y.; Lu, C.; Jiang, X. Multiplexed Random Access Approach to DNA Microspheres for High-Capacity Data Storage. *Adv Funct Mater* **2024**, *34*, doi:10.1002/adfm.202408852.
15. Mo, F.; Li, C.; Sun, J.; Lin, X.; Yu, S.; Wang, F.; Liu, X.; Li, J. Programming Fast DNA Amplifier Circuits with Versatile Toehold Exchange Pathway. *Small* **2024**, *20*, doi:10.1002/smll.202402914.
16. Stanisavljevic, M.; Krizkova, S.; Vaculovicova, M.; Kizek, R.; Adam, V. Quantum Dots-Fluorescence Resonance Energy Transfer-Based Nanosensors and Their Application. *Biosens Bioelectron* **2015**, *74*, 562–574, doi:https://doi.org/10.1016/j.bios.2015.06.076.
17. Liu, M.L.; Chen, B. Bin; Li, C.M.; Huang, C.Z. Carbon Dots: Synthesis, Formation Mechanism, Fluorescence Origin and Sensing Applications. *Green Chemistry* 2019, *21*.
18. Zuo, P.; Lu, X.; Sun, Z.; Guo, Y.; He, H. A Review on Syntheses, Properties, Characterization and Bioanalytical Applications of Fluorescent Carbon Dots. *Microchimica Acta* 2016, *183*.
19. Yukawa, H.; Baba, Y. In Vivo Fluorescence Imaging and the Diagnosis of Stem Cells Using Quantum Dots for Regenerative Medicine. *Anal Chem* 2017, *89*.
20. Lin, M.; Lee, J.U.; Kim, Y.; Kim, G.; Jung, Y.; Jo, A.; Park, M.; Lee, S.; Lah, J.D.; Park, J.; et al. A Magnetically Powered Nanomachine with a DNA Clutch. *Nat Nanotechnol* **2024**, *19*, doi:10.1038/s41565-023-01599-6.
21. Meng, L.; Sun, M. Tip-Enhanced Photoluminescence Spectroscopy of Monolayer MoS_2. *Photonics Res* **2017**, *5*, doi:10.1364/prj.5.000745.
22. Lin, Y.; Hu, J.; Zhang, W.; Jiang, L.; Yi, D.; Rujiralai, T.; Ma, J. Broadband Single-Molecule Fluorescence Enhancement Based on Self-Assembled Ag@Au Dimer Plasmonic Nanoantennas. *Nanoscale* **2022**, *14*, doi:10.1039/d2nr03466b.
23. Li, J.F.; Li, C.Y.; Aroca, R.F. Plasmon-Enhanced Fluorescence Spectroscopy. *Chem Soc Rev* 2017, *46*.
24. Raab, M.; Jusuk, I.; Molle, J.; Buhr, E.; Bodermann, B.; Bergmann, D.; Bosse, H.; Tinnefeld, P. Using DNA Origami Nanorulers as Traceable Distance Measurement Standards and Nanoscopic Benchmark Structures. *Sci Rep* **2018**, *8*, doi:10.1038/s41598-018-19905-x.
25. Lo, P.K.; Karam, P.; Aldaye, F.A.; McLaughlin, C.K.; Hamblin, G.D.; Cosa, G.; Sleiman, H.F. Loading and Selective Release of Cargo in DNA Nanotubes with Longitudinal Variation. *Nat Chem* **2010**, *2*, doi:10.1038/nchem.575.
26. Ren, S.; Ren, L.; Wei, B.; Liu, Y.; Yang, J.; Li, J.; Wang, L. DNA-Templated Fabrication of Metal Nanostructures with Special Shapes. *Advanced Sensor and Energy Materials* **2024**, 100133, doi:10.1016/j.asems.2024.100133.
27. Cecconello, A.; Cencini, A.; Rilievo, G.; Tonolo, F.; Litti, L.; Vianello, F.; Willner, I.; Magro, M. Chiroplasmonic DNA Scaffolded "Fusilli" Structures. *Nano Lett* **2024**, *24*, 5944–5951, doi:10.1021/acs.nanolett.3c04943.
28. Su, Q.; Jiang, C.; Gou, D.; Long, Y. Surface Plasmon-Assisted Fluorescence Enhancing and Quenching: From Theory to Application. *ACS Appl Bio Mater* **2021**, *4*, 4684–4705, doi:10.1021/acsabm.1c00320.
29. Lu, G.; Zhang, T.; Li, W.; Hou, L.; Liu, J.; Gong, Q. Single-Molecule Spontaneous Emission in the Vicinity of an Individual Gold Nanorod. *Journal of Physical Chemistry C* **2011**, *115*, doi:10.1021/jp203317d.

 doi:10.20944/preprints202502.0204.v1

30. Mertens, H.; Koenderink, A.F.; Polman, A. Plasmon-Enhanced Luminescence near Noble-Metal Nanospheres: Comparison of Exact Theory and an Improved Gersten and Nitzan Model. *Phys Rev B Condens Matter Mater Phys* **2007**, *76*, doi:10.1103/PhysRevB.76.115123.